STRUCTURE AND OXIDATION BEHAVIOR OF ZIRCONIUM-BASE ALLOYS

L. V. Ramanathan
Instituto Pesquisa Energeticas e Nucleares
Sao Paulo, Brasil

ABSTRACT

The influence of 2.5% and 5.1% Nb additions to Zr and 0.05% to 0.26% C additions to zircaloy-2 on the structure and oxidation behavior of the Zr-base alloys have been studied. Increase in the cooling rates of Zr-base alloys from the β-phase and $(\alpha+\beta)$ phase regions resulted in increased tendency for a basket weave type of martensitic structure. Increasing C in zircaloy-2 reduced the size of the α-grains in specimens cooled from the and β-phase regions. Etching studies on zircaloy-2 have shown that carbides were etched in very dilute etchants, whereas regions very close to and a certain distance away from the carbides were preferentially attacked in stronger etchants. Isothermal oxidation measurements on the various Zr-base alloys indicated increasing oxidation rates with alloying/impurity elements. A decrease in time to transition with increasing C and Nb contents has also been observed. EPMA studies across metal and oxide on Zr-Nb alloys revealed a sharpe drop in Zr content across the interface.

INTRODUCTION

The use of zirconium and its alloys in the nuclear industry is quite widespread, and is mainly due to the low absorption cross section of Zr for thermal neutrons, its mechanical strength and resistance to corrosion. A number of Zr-base alloys containing different alloying elements are in use, and their structural as well as oxidation behavior have been fairly well investigated. LeSurf et al.(1) reported an increase in the mechanical properties of Zr alloys that were quenched from the $(\alpha+\beta)$-phase regions. Marked increases in corrosion resistance of Zr alloys heat treated in the $(\alpha+\beta)$-zones have also been observed(2).

Porte et al.(3) studied the kinetics of oxidation of Zr-C alloys and reported breakaway oxidation in the case of high C containing Zr alloys. In Zr-C alloys (with 0.05% C) Misch and Van Drunen (4) observed breakaway oxidation only after extended times. Chauvin et al.(5) investigated the oxidation of Zr-C alloys in oxygen at 600-900° C and attributed the enhanced rate to preferential oxidation of carbide inclusions which formed pimples of white oxide that burst due to accumulated CO_2 within the oxide layer; thus producing breakaway. The high oxidation rate of Zr-C alloys in dry oxygen has been attributed by Ahmed et al.(6) to rapid attack of the regions adjacent to carbides. More recent studies (7) on the oxidation of fused carbides revealed that oxidation rates increased with decreasing carbon content.

Zr-2.7%Nb alloys oxidised in the range 650-1000° C were found to obey parabolic rate laws of oxidation. Dawson et al.(8) reported selective oxidation of Nb from the dispersed high Nb containing phase to Nb_2O_5. In Zr-Nb alloys, at oxidation temperatures beyond 450-700° C, Klepfer (9) found the influence of Nb on Zr to be detrimental in terms of oxidation rates. Porte et al.(3) concluded from their oxidation measurements on various Zr-Nb alloys that an increase in Nb content from 0.6 to 3.82% decreased the time to transition from 365 to 49 minutes. In this work, in order to further elucidate reported results, the influence of an impurity agent such as C in zircaloy-2, and a solute element such as Nb in Zr on the structure and oxidation behavior have been investigated.

EXPERIMENTAL

Specimen preparation

Zr-2.5%Nb specimens 3mm×5mm×3mm and of nominal composition were cut with an Isomet cutter from sheets supplied by Wang Teledyne and annealed in an argon atmosphere. Zr-5.1%Nb alloy was prepared in a vacuum arc furnace by melting together Zr-2.5%Nb and pure Nb. The ingot was homogenised, rolled, and specimens of approximately the above mentioned dimensions were cut and annealed. All the specimens were degreased in acetone, followed by CCl_4, rinsed in deionized water and dried.

Zircaloy-2 specimens containing different amounts of C were obtained by hot pressing zircaloy-2 powder ($\simeq 44\mu$) at 1200° C and 53.9MNm^{-2} in graphite dies for 10, 30, 120 and 240 minutes. Two hot pressed compacts were prepared under each set of conditions and a compact from each batch was homogenised at 1000° C in argon for several hours to distribute the carbon. Subsequently, specimens were cut from each of the compacts for analysis, microstructural studies and oxidation measurements. The carbon contents and designation of the compacts are shown in Table I. Degreasing and cleaning of the specimens were carried out as mentioned before.

TABLE-I

Designation	Hot pressing time (minutes)	C content(%)
A	10	0.05
B	30	0.10
C	120	0.201
D	240	0.260

Structure studies

Specimens of Zr-Nb and zircaloy-2 C were solutionised for 10 to 15 minutes in the β-phase region and (a) cooled rapidly and (b) cooled slowly. One set of specimens were similarly maintained in the (α + β) - phase region and cooled at the two different rates. The specimens were then mounted, abraded, polished electrochemically, etched in a very dilute mixture of 50:50 of 0.1HF and 0.1HNO_3 and examined microscopically.

Oxidation studies

The specimens were oxidised in a 951 Dupont Thermogravimetric Analyzer operated in conjunction with a 900 Dupont Thermal Analyzer. Isothermal oxidation was carried out in flowing oxygen at different temperatures ranging from 500-800° C. Isothermal weight gain curves were recorded continuously with the Thermal Analyzer.

After oxidation, the specimen surfaces were examined with an optical microscope. An oxidised specimen from each batch was also mounted in section and its structure examined. A Cambridge electron probe microanalyzer was used to analyse for Zr and Nb across the oxide sections on oxidised Zr-Nb alloys.

RESULTS AND DISCUSSIONS

Metallographic studies

Zircaloy-2+C. The influence of C on the microstructure of zircaloy-2 can be seen from figures 1a-1d. An increase in C content from 0.1% to 0.20% (figures 1a and 1b) results in an increase in the number of grains. Similar variations in microstructure between specimens taken from the middle and end of unhomogenised hot pressed compacts have been observed. These differences in the structure could be attributed to significant variations in the carbon content. Also, differences in the microstructure between figures 1a and 1c as well as between figures 1b and 1d indicate the influence of cooling rate from 1100°C the β - phase region. Predictably slow cooling results in the formation of large but less number of grains, and rapid cooling in a large number of small grains. Rapid cooling of zircaloy-2 + 0.1%C from 850°C (α + β)-phase region rendered the type of structure shown in fig. 1e. Upon comparing figs. 1a and 1e, the differences between reprecipitation of α throughout the structure, and reprecipitation in only some portions can be seen.

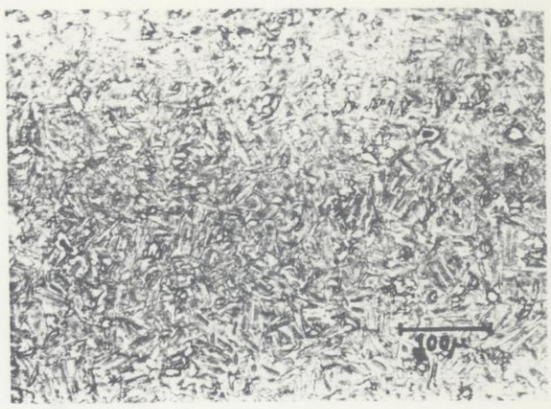

(b)

(c)

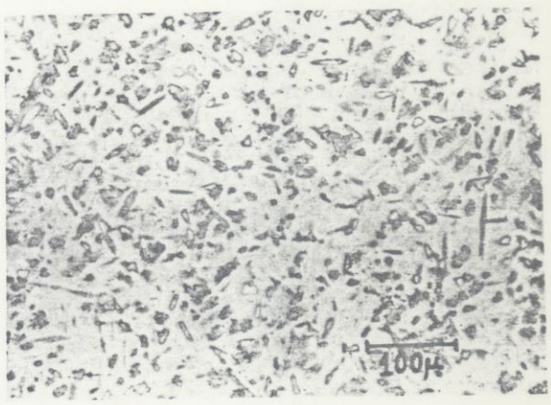

(d)

Figure 1. Microstructure of zircaloy-2+C
(a) 0.1%C, rapidly cooled from β -phase.
(b) 0.2%C, rapidly cooled from β -phase.
(c) 0.1%C, slowly cooled from β -phase.
(d) 0.2%C, slowly cooled from β -phase.

The nucleation and growth of the α-phase from the β-phase depends upon the number and distribution of nucleation sites. Since C has no solid solubility in either the α or the β-phase-Zr, the carbides, along with the intermetallic precipitates, act as the predominant nucleation sites for the α-phase. The structure in fig. 1b results when a greater number of such nucleation sites are available, in comparison to the structure in fig. 1a.

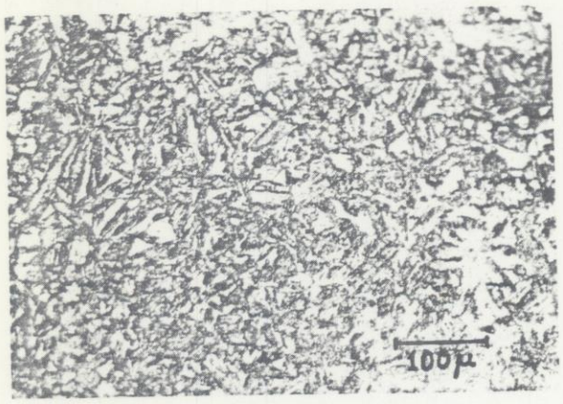

Figure 1e. Microstructure of zircaloy-2+0.1%C rapidly cooled from the ($\alpha+\beta$)-phase.

A region close to the edge of a non-homogenized compact reheated into the ($\alpha+\beta$) phase region and cooled, is shown in fig.2a. Continuous white lines of zirconium carbides are revealed. Regions close to the carbides can be seen to be heavily etched, whereas regions further away are not so heavily etched. Similar observations were reported by Cox (10). Upon repolishing the specimen shown in figure 2a, and etching in a more dilute HF/HNO_3 mixture, a different structure as shown in figure 2b was revealed. Here the carbides have been attacked preferentially, while the surrounding areas remained unattacked. This change in etching behavior suggests that the preferential dissolution of C containing regions in zircaloy-2 are dependent on the nature of the etchant. In very dilute etchants the carbides are susceptible to dissolution, while the C containing regions in the vicinity of the carbides are passive. However, in more concentrated etchants, and after longer periods of attack, the regions surrounding the carbides are more prone to attack. The C concentration gradient gives rise to the different grades of etching.

Zirconium-niobium alloys. A comparison between figures 3a and 3b reveals that rapid cooling of Zr-2.5%Nb from 750°C,(α + β)phase region, gave rise to fibrous structure whereas slow cooling rendered a more homogeneous structure (fig,3a). The Zr-5.1%Nb alloy slowly cooled however, resulted in a fibrous structure, and rapid cooling in parallel plate type of structure. The change in cooling rate, rapid to slow for Zr-2.5% b from 900°C,β-phase region temperature, resulted in a structural change basketweave type to parallel plate type respectively,(figures 3c and 3d). Upon increasing the Nb content to 5.1%, the grain size increased if β-phase temperature and cooling rate were maintained constant. The above dependence of structure on cooling rate from β-phase is due to increased available nucleation sites for the basketweave type of structure and few sites for the parallel plate type of structure. Similar observations were reported by Ökvist and Källstrom(11).

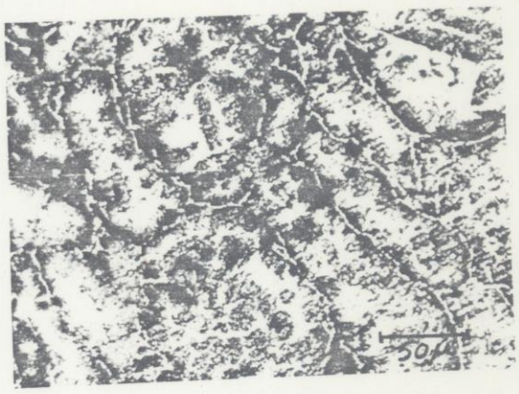

Figure 2a. Microstructure of zircaloy-2+0.2%C etched in 50:50::0.1MHF:0.1MHNO_3.

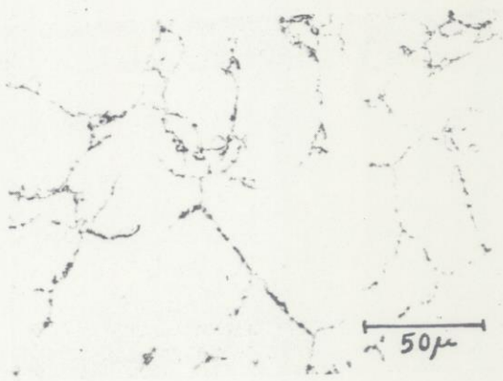

Figure 2b. Microstructure of zircaloy-2+0.2%C etched in extremely dilute HF/HNO_3 mixture.

Oxidation measurements

Weight gain vs time curves were recorded continously with the Thermogravimetric analyzer after an initial 10 minutes equili-bration period. during which time, most of the influences of differences in specimen history were kept to a minimum due to identical specimen preparation procedures. The results of isothermal oxidation of the various zircaloy-2 and Zr-Nb specimens are shown in figures 4 and 5. The weight gain is attributable primarily to the interaction between Zr and oxygen to form the metal dioxide. In the pre-transition zone, oxide growth is mainly due to oxygen ion diffusion

(a)

(b)

Figure 3. Microstructure of Zr-2.5%Nb alloy.
(a) slowly cooled from the $(\alpha+\beta)$ phase
(b) rapidly cooled from $(\alpha+\beta)$-phase.

(c)

(d)

Figure 3(c) Microstructure of Zr-2.5%Nb alloy slowly cooled from β-phase.
(d) rapidly cooled from β-phase.

through the oxide film to the metal-oxide interface(6). These have been confirmed by direct observations using inert markers on Zr during oxidation(12).

The changes in oxidation behavior with C content in the low temperature region revealed no appreciable difference in rate. However at higher temperatures, an initial slow rate of oxidation was followed by a quicker rate, rendering thereby a transition inrate as seen in figure 4. The oxide formed initially was dark, and became the well adherent black ZrO_2. The change in oxidation rate coincided with the formation of localised spots of cracks on the black oxide. Formation of an oxide of Zr with a different stoichiometric composition took place at these spots (12). The latter oxide was poorly adherent and grey to white in colour. The localised spots of cracked white oxide had the appearence of nodules. With time at temperature, the white oxide spread until the whole surface became covered. Non homogenized specimens of zircaloy-2+C when oxidised at the higher temperatures (600-800° C) revealed a very large number of white oxide nodules close to the periphery of the specimen. Since most of the C was present in regions close to the periphery in nonhomogenized specimens, it is reasonable to assume that the nucleation of the white oxide nodules were aided by the presence of the carbides of zirconium. It can also be seen from figure 4. that in the post-transition zone, an increase in the C content increases the oxidation rate at all temperatures.

The absence of solid solubility of C in Zr results in the formation of the intermetallic $ZrC_{0.58}$ (13), which precipitates along grain boundaries. The oxide film on the surface of such intermetallic compounds probably has a structure slightly different from that on the other areas, that are formed in accordance with different laws, and hence do not match well with the surrounding oxide. This mismatch probably leads to the cracking observed. Also in the case of C containing zircaloy-2, the transition point is earlier than in pure zircaloy-2, and may be attributed to the above reason.

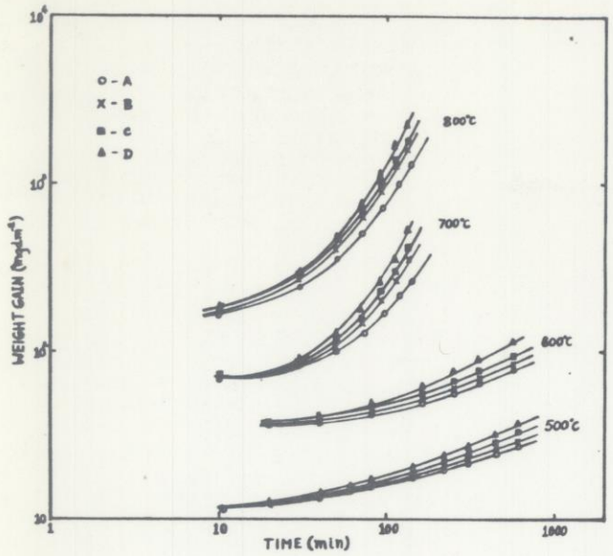

Figure 4. Isothermal weight gain vs time curves for zircaloy-2+C oxidised at 500-800° C.
o-0.05%C, x -0.1%C, ■ -0.201%C, ▲-0.26%C.

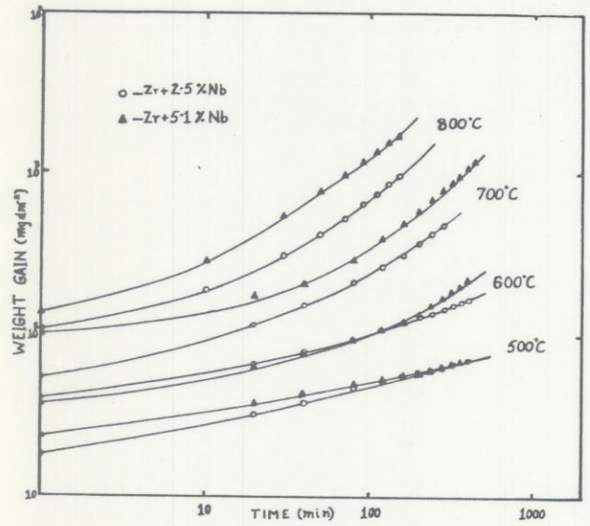

Figure 5. Isothermal weight gain vs time curves for Zr-Nb alloys oxidised at 500-800° C.

The influence of Ccontent on the time to transition for zircaloy-2 is shown in figure6. With increasing C the time to transition decreases, and may be attributed to an increase in the number of foci for oxide crack initiation. At 800° C, the dependence of time to transition on C content is not so clearly seen due to the short time to breakdown of oxide.

Figure 5 shows the oxidation behavior of the two Zr-Nb alloys. Observations similar to those made with zircaloy-2 have been obtained.

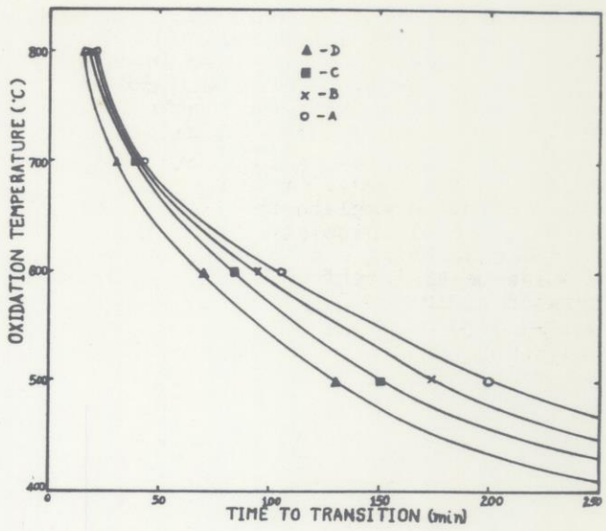

Figure 6. Influence of C content of zircaloy-2 on time to transition of oxidation.
o-0.05%C, x-0.1%C, ■ -0.201%C and ▲-0.26%C.

An initial slow oxidation rate is followed by an increased rate, and corresponding to this rate change, the black ZrO_2 changes to white ZrO_2, although no nodule formation was observed. All specimens oxidised at temperatures $>$ 700° C revealed cracked oxide surfaces (figure 7).

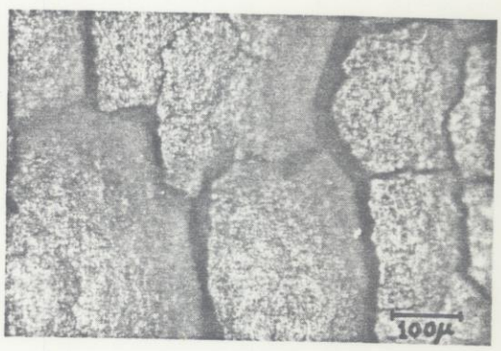

Figure 7. Microstructure of cracked oxide on Zr-2.5%Nb alloy, oxidised at 700° C.

An increase in oxidation rate with Nb content for all oxidation temperatures can also be seen from figure 5. The Zr-5.1%Nb alloy reached transition earlier, and this may be attributed to easier paths for the migration of the reactive species. The paths are probably provided by misorientations in the oxide grains.

Previous investigations(10,14), have reported a number of transition points, or even a transition zone during oxidation of Zr-base alloys. In this investigation, a single transition only has been observed in the temperature range 600-800° C. At lower temperatures, due to the reduced duration of

the test, transition had not set in. The observed single transition may be attributed to the formation of cracked white oxide that spread with concomitant increase in oxidation rate, brought about by easier access for the oxygen migrating through the cracks in the oxide. In zircaloy-2 and Zr-Nb alloys, the cracking of the oxide is due probably to stresses in the oxide. Other opinions however exist to explain the transition behavior, one of which attributes the transition as being due to lateral cracks at the oxide-metal interface, caused by the stress generated during oxide growth(15).

Surface studies on oxidised specimens

Optical microscopic studies on the oxidised zircaloy-2+C and Zr-Nb alloy specimens revealed some interesting features. All the specimens oxidised at the temperatures upto 500° C revealed the black and adherent oxide. Visual examination of the specimens oxidised for about 400 minutes at 600° C revealed the white oxide only at regions near the edges. However under the microscope, the oxide away from the edges was also cracked. Specimens oxidised at higher temperatures had heavily cracked white oxide covering the entire surface (figure6). Examination of oxidised metal sections showed variations in oxide thickness on different grains, attributable to differences in surface activity of individual grains.

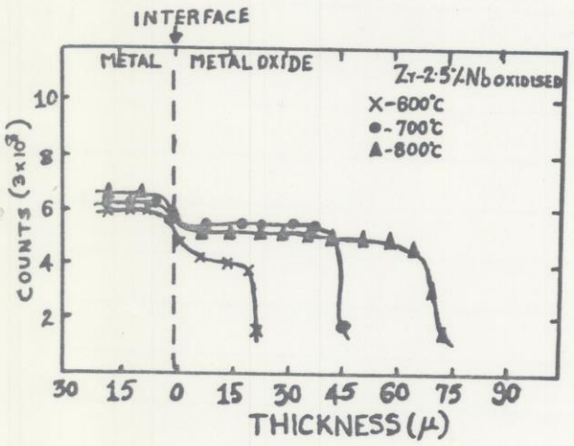

Figure 8. Variation of Zr content in metal and oxide in Zr-2.5%Nb alloy oxidised at 600-800° C.

Electron probe microanalysis scans for Zr and Nb on oxidised Zr-Nb alloys revealed changes in the Zr and Nb contents across the metal and metal oxide. The main observations were: (i) a significant drop in Zr content across metal/metal oxide interface (figure 8), (ii) uniform Zr content across the oxide, and (iii) large variations in the Nb content in the metal as well as the oxide. The variations in the Nb content are possibly due to tempering effects during oxidation, and segregations in the oxide.

CONCLUSIONS

1. An increase in the C content of zircaloy-2 was found to decrease average grain size, but increase the number of grains per unit area. Carbides were found along grain boundaries nearthe edges in non-homogenized specimens.
2. Rapid cooling of both zircaloy-2+C and Zr-Nb alloys from the β-phase region resulted in a Widmanstätten structure. Slow cooling rates rendered fewer but larger number of grains. Cooling from the $(\alpha+\beta)$-phase region resulted in more homogeneous structures.
3. Oxidation of zircaloy-2+C and Zr-Nb alloys at temperatures $> 600°$ C revealed a single rate transition. In the pre-transition region black uncracked ZrO_2 formed. The transition in rate coincided with the appearance of white oxide nodules on zircaloy-2+C, and white oxide only on Zr-Nb alloys, that spread throughout the surface.
4. Oxidation of zircaloy-2+C and Zr-Nb alloys in the temperature range 500-800° C showed distinct increases in the oxidation rate with impurity/solute element.
5. The time to transition has been found to decrease with increasing oxidation temperature and increasing impurity/solute element.
6. The high C containing regions along the edge in non-homogenized zircaloy-2 specimens were prone to quicker oxidation and transition.

REFERENCES

1. LeSurf, J.E., Applications-Related Phenomenon in Zirconium and its alloys. 286 (1969)
2. Ahmed, T., Metals 77: The 30th annual Conference of the Australian Inst. of Metals. 3B1-3B2, (1977).
3. Porte, H.A., Schnizlein, J.G., Vogel, R.C., Fisher, D.F., J. Electrochem. Soc. 107, 506, (1960).
4. Misch, R.D., and Van Drunen. C., Proc of U.S. At. Energy Comm., Symp. on Zr alloy developement GEAP4089 USAEC, Vol II (1962).
5. Chauvin, G., Boudoresque, B., Coriou, H., Hure, J., Rev. Mett., 55, 939, (1958).
6. Ahmed, T., Keys, L.J., and Wallwork, G.R., J. Less Com. Metals, 33, 369, (1973).
7. Stepanchuk, A.N., Trukhan, S.G., and Shlyuko, V.Ya., Ogneupory, 4, 42, (1975).
8. Dawson, J.K., et al.-p 158, Proc III U.N. Int. Conf. on Peaceful uses of Atomic Energy, Geneva (1964)
9. Klepfer, H.H., Report USAEC GEAP 4284, (1963).
10. Cox, B., Corrosion, 16, 4, 124, (1960).
11. Okvist, G., and Kallstrom, K., J. of Nucl. Materials, 35, 316, (1970).
12. Parfenov, B.G., Gerasimov, V.V., Venediktova, G.I., Corrosion of Zr and Zr alloys, Atomizdat, Moscow, (1967).
13. Storms, E.K., The Refractory Carbides, Academic Press, New York, (1967).
14. Coriou, H., Gauduchau, J., Grall, L., and Hure, J., Mem. Sci. Rev. Metall, 56, 693, (1959).
15. Bradhurst, D.H., and Heuer, P.M., Journal of Nuclear Materials, 37(1), 35, (1970).